Supporting Information For:

CO_2 Reduction under Periodic Illumination of ZnS

Article permalink: http://dx.doi.org/10.1021/jp4126039

Publication date: May 12, 2014

*Ruixin Zhou and Marcelo I. Guzman**

Department of Chemistry, University of Kentucky, Lexington, Kentucky 40506, Unites States

*Corresponding author's email: marcelo.guzman@uky.edu

The Journal of Physical Chemistry C

Content **Pages**

Additional Results and Discussion

Crystal Structure and Properties of ZnS.

The crystal structure of fresh and photo-processed ZnS dried under vacuum was identified by powder X-ray diffraction (XRD) with a D8 Advance Bruker AXS (Cu K_α radiation, $\lambda = 1.5418$ Å) diffractometer. XRD data from 10° to 80° was collected at a scan rate of 1° min^{-1}, background corrected by subtracting the signal of the empty sample holder, and normalized to the maximum sample intensity. In addition of providing confirmation of the crystal structure of dry ZnS by XRD, Raman Spectroscopy was also used (see below). The XRD patterns of the synthesized colloidal particles before and after 1, 2, and 3 hours of irradiation appears to be identical (Figure S1A-D). ZnS remains in the pure cubic sphalerite phase for nanocrystallites that produce broad spectral peaks. The peaks at 2θ values of 28.71°, 47.95°, and 56.80° correspond to the respective crystal planes (111), (220), and (311) of faced centered cubic ZnS (JCPDS No. 00-005-0566).

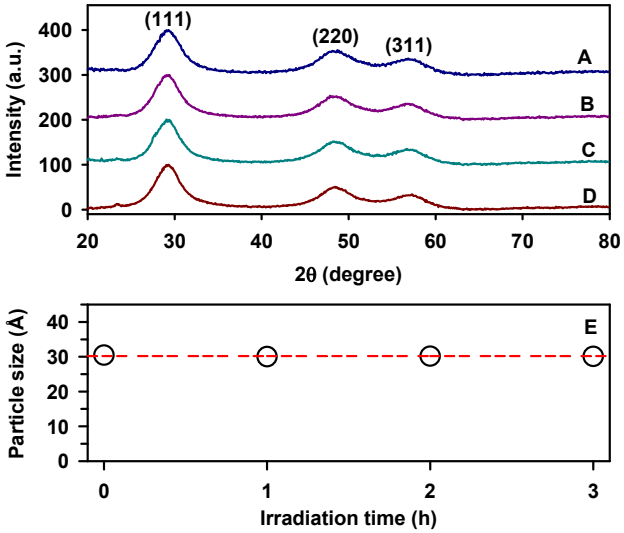

Figure S1. XRD patterns for ZnS (A) before and after (B) 1, (C) 2, and (D) 3 hours of irradiation. (E) Particle size vs. irradiation time from Scherrer's equation for the peak at 28.71° (D = 30.19 ± 0.19 Å).

The lattice constant a = 5.381 Å calculated from the (111) plane of freshly synthesized ZnS is within the error range of the standard literature value (a = 5.406 Å). Applying the Scherrer equation for submicrometer size particles, $D = k\,\lambda/(\beta \cos\theta)$, to the full width at half maximum (FWHM) of the (111) peak in Figure S1A-D, the average grain size of the nanocrystallites is D = 30.19 ± 0.19 Å. The Scherrer constant used is k = 0.9, λ is the wavelength of the Cu K_α line applied, β is the FWHM of the peak in radians, and θ is the diffraction angle of the (111) peak. The diameter remains practically constant before and after irradiation (Figure S1E). The absence of any wurtzite ZnS structure is expected because this hexagonal phase requires a synthesis at higher temperature and pressure. A comparison of panels A-D in Figure S1 indicates that the crystal phase and size of ZnS remains identical during the reaction.

Analysis by nitrogen adsorption–desorption isotherms at 77 K with the Brunauer-Emmett-Teller (BET) method (Micromeritics ASAP 2020 Physisorption Analyzer) was performed for samples before and after 1 h of irradiation with the total output of the UV lamp. Although dry ZnS may not be representative of the actual conditions of the catalyst in water, the small variation of the specific surface area and total pore volume of both samples suggests the system was stable during the reaction. A small 5% change is observed in the BET surface areas for the ZnS colloidal suspensions before (180 $m^2\ g^{-1}$) and after 1 h of UV irradiation (190 $m^2\ g^{-1}$). Similarly, the total pore volume of ZnS remained within a 3% difference before irradiation (0.102 $cm^3\ g^{-1}$) and after 1 h photolysis (0.105 $cm^3\ g^{-1}$).

A Raman microscope (DXR, Thermo Scientific) registered the Raman spectra of samples mounted and dried under a nitrogen atmosphere on glass slides by applying 5 mW (λ_{laser} = 532 nm) to register 128 scans with 2 cm^{-1} resolution. Figure S2 shows the Raman spectra of ZnS in the cubic phase, in agreement with the XRD data in Figure S1. The main Raman lines in Figure

S2A occur at 269, 349, 423, and 612 cm^{-1}, and they are associated to the transverse optical phonon (TO) at the Γ point, the longitudinal optical phonon (LO) at the Γ point, the sum combination bands for the LO and the transverse acoustic phonon (LO + TA), and the overtone from the combination of two different TO phonons.[1] The oxidation of sulfide hole scavenger during the reaction produces a small amount of yellow colloid during irradiation, identified as elemental (rhombic) sulfur, S_8, in the Raman spectrum (Figure S2B-D). This species is not derived from the catalyst that remains intact as shown by XRD and TEM data. Rhombic sulfur is as an oxidation intermediate produced by the sulfide hole scavenger with Raman peaks at 220, 439 and 473 cm^{-1} that become more intense with longer irradiation time. The three peaks differ less than ±2 cm^{-1} from the previous assignment for the Raman active species of molecular S_8 with D_{4d} symmetry.[2]

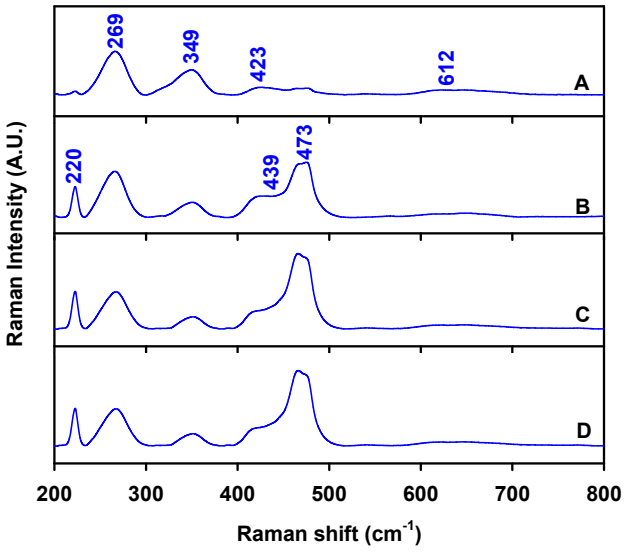

Figure S2. Raman spectra (λ_{laser} = 532 nm) for an experiment with a colloidal suspension of ZnS (A) before and after (B) 1, (C) 2, and (D) 3 hours of irradiation.

Since the XRD measurements showed that the crystallites phase and grain size were not significantly affected during photolysis, the particle sizes and morphologies before and after irradiation were expected to be similar. Thus, only freshly synthesized ZnS samples were

analyzed by transmission electron microscopy (TEM). Samples for TEM were transferred to a 300-mesh Formvar-carbon coated copper grid and dried under nitrogen gas. The morphology of highly dispersed ZnS nanoparticles on the copper grid was visualized by TEM in a JEOL 2010F field emission electron microscope. The JEOL 2010F unit equipped with an Oxford INCA detector also provided energy-dispersive X-ray spectroscopy (EDS) measurements.

The TEM images in Figures S3A and B show aggregates of irregular shaped fine nanoparticles. Integration of the areas under the *K* lines in the EDS spectrum of Figure S3C indicates that the precipitated colloids are comprised of Zn and S elements with a Zn:S percentage ratio of 50.9:49.1. This ratio agrees with the 1:1 stoichiometry expected from the synthesis, and was also observed after one hour of irradiation. The presence of elemental C and Cu is due to the carbon coated copper grid used to hold the nanoparticles as confirmed by registering its EDS spectrum alone. A trace of oxygen peak (not indicated) in the EDS spectrum probably originates from the unavoidable surface-adsorption of oxygen onto the samples from exposure to air during sample processing.

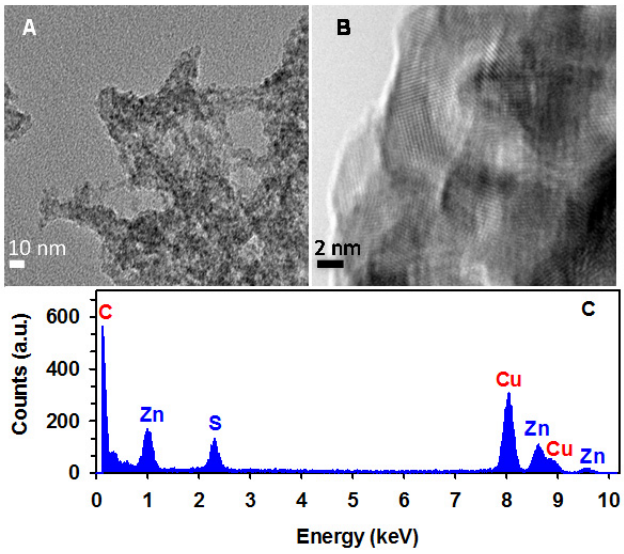

Figure S3. TEM images of ZnS with a scale of (**A**) 10 nm and (**B**) 2 nm. (**C**) EDS spectrum of ZnS.

Control experiments (Table S3) confirm that the production of formate is due to the irradiation of the ZnS colloidal suspension in the presence of sulfide hole scavenger.

Figure S4 shows the photoluminescence spectrum of a colloidal suspension of ZnS excited at λ_{exc} = 300 nm, which contains a broad peak centered at ${}^{M}\lambda_{em}$ =420 nm maximum emission wavelength. The plot to the left of Figure S4 contains the integrated photoluminescence intensity (area under the emission curve) for excitation wavelengths, λ_{exc}, values of 290, 300, 305, 310, 320, and 330 nm. The largest emission area in Figure S4 corresponds to a maximum excitation wavelength ${}^{M}\lambda_{exc}$ = 300 nm, which agrees well with the reflection edge observed for ZnS powder in Figure 5 of the main text. The observed photoluminescence band with ${}^{M}\lambda_{em}$ =420 nm, and FWHM of ~85 nm, originates from the recombination of electrons and holes in trapped surface states located in the forbidden region of the bandgap due to sulfur vacancies.[3] This photoexcited ZnS* decays a 90% within $\tau_{\lambda_{em}=420\,\mathrm{nm}}$ ~30 ns.[4] The emission in the photoluminescence spectrum is Stokes shifted by ~108 nm with respect to the absorption band edge in Figure 5 (λ = 312 nm).

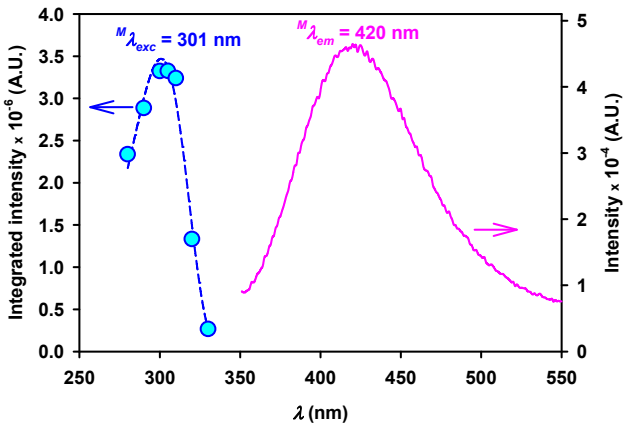

Figure S4. Photoluminescence spectrum of colloidal ZnS suspension excited at λ_{exc} = 300 nm (pink trace and right axis) and integrated photoluminescence intensities for 290 ≤ λ_{exc} ≤ 320 nm (blue circles and left axis).

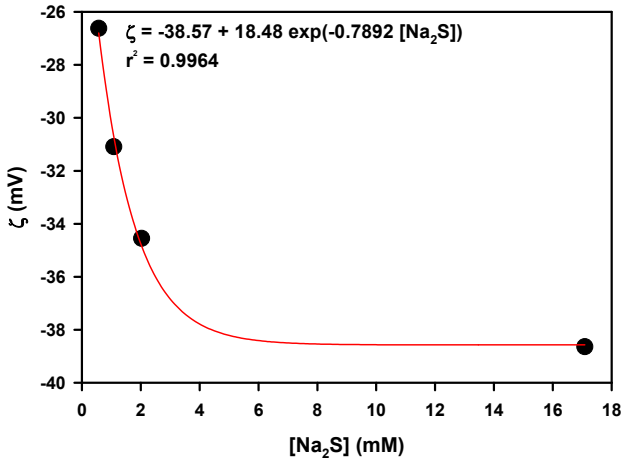

Figure S5. Zeta-potential (ζ) vs. increasing [Na_2S] for undiluted samples under the same experimental conditions of Figure 7 (pH = 7.0). The red line shows the nonlinear least square regression for the equation given in the plot.

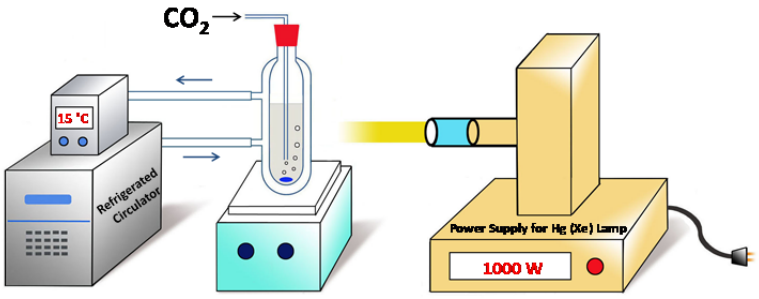

Scheme S1. Simplified diagram of photochemical setup.

Table S1. Reduction potentials for some half-reactions of interest

Reduction half-reaction	$E^{o}_{1/2}$ (V)	Ref.
$\emptyset_{\mathrm{ZnS}} + e^{-} \rightleftharpoons e^{-}_{\mathrm{CB(Zns^{-})}}$	-1.04	[5]
$CO_2(g) + H^+ + 2\ e^- \rightleftharpoons HCOO^-$	-0.29	[6]
$2\ SO_4^{2-} + 2\ e^- + 4\ H^+ \rightleftharpoons S_2O_6^{2-} + 2\ H_2O$	-0.25	[7]
$SO_4^{2-} + 2\ e^- + 2\ H^+ \rightleftharpoons SO_3^{2-} + H_2O$	-0.10	[8]
$2\ H^+ + 2\ e^- \rightleftharpoons H_2$	0.00	[6]
$S_2O_6^{2-} + 2\ e^- \rightleftharpoons 2\ SO_3^{2-}$	0.04	[7]
$S(s, rhombic) + 2\ e^- + 2\ H^+ \rightleftharpoons H_2S(aq)$	0.17	[6]
$SO_4^{2-} + 8\ e^- + 9\ H^+ \rightleftharpoons HS^- + 4\ H_2O$	0.25	[6]
$2\ SO_4^{2-} + 8\ e^- + 10\ H^+ \rightleftharpoons S_2O_3^{2-} + 5\ H_2O$	0.29	[8]
$SO_4^{2-} + 8\ e^- + 10\ H^+ \rightleftharpoons H_2S(aq) + 4\ H_2O$	0.31	[6]
$SO_4^{2-} + 6\ e^- + 8\ H^+ \rightleftharpoons S(s, rhombic) + 4\ H_2O$	0.36	[6]
$h^{+}_{VB(ZnS^{+})} + e^{-} \rightleftharpoons \emptyset_{\mathrm{ZnS}}$	2.55	[5]

Reduction potentials for standard states versus the normal hydrogen electrode (NHE). The relationship $E^{o}_{1/2}$= 0.05916 pe^{o} was used to convert the reference values.[6,8]

Table S2. Electrons loss by sulfide sequential oxidation at the valence band of ZnS

Initial oxidation state		Intermediate or final oxidation state				
		0	+II	+IV	+V	+VI
		S	$S_2O_3^{2-}$	SO_3^{2-}	$S_2O_6^{2-}$	SO_4^{2-}
-II	S^{2-}	-2	-4	-6	-7	-8
0	S		-2	-4	-5	-6
+II	$S_2O_3^{2-}$			-2	-3	-4
+IV	SO_3^{2-}				-1	-2
+V	$S_2O_6^{2-}$					-1

Table S3. Experiments and controls to demonstrate the heterogeneous production of formate

	Conditions				Product
	ZnS	UV	CO_2	Hole scavenger	$HCOO^-$
Experiment	+	+	+	+	+
Control A	−	+	+	+	−
Control B	+	−	+	+	−
Control C	+	+	−	+	−
Control D	+	+	+	−	−

Table entries of "+" and "−" indicate the presence or absence of a species, respectively.

References

(1) Nilsen, W. G. Raman Spectrum of Cubic ZnS. *Phys. Rev.* **1969**, *182*, 838-850.

(2) Scott, D. W.; McCullough, J. P.; Kruse, F. H. Vibrational Assignment and Force Constants of S_8 from a Normal-coordinate Treatment. *J. Mol. Spectrosc.* **1964**, *13*, 313-320.

(3) Denzler, D.; Olschewski, M.; Sattler, K. Luminescence studies of localized gap states in colloidal ZnS nanocrystals. *J. Appl. Phys.* **1998**, *84*, 2841-2845.

(4) Henglein, A.; Gutiérrez, M. Photochemistry of Colloidal Metal Sulfides. 5. Fluorescence and Chemical Reactions of ZnS and ZnS/CdS Co-Colloids. *Berich. Bunsen. Gesell.* **1983**, *87*, 852-858.

(5) Xu, Y.; Schoonen, M. A. A. The Absolute Energy Positions of Conduction and Valence Bands of Selected Semiconducting Minerals. *Am. Mineral.* **2000**, *85*, 543-556.

(6) Stumm, W.; Morgan, J. J. *Aquatic Chemistry*, 3rd ed.; John Wiley & Sons: New York, 1996.

(7) Board, A. J.; Parsons, R.; Jordan, J. *Standard Potentials in Aqueous Solution*, 1st ed.; CRC Press: New York, 1985.

(8) Morel, F. M. M.; Hering, J. G. *Principles and Applications of Aquatic Chemistry*; John Wiley & Sons: New York, 1993.